Multi-mode coupling analysis of a sub-terahertz band planar corrugated Bragg reflector*

Liu Guo(刘 国)†, Luo Yong(罗 勇), Wang Jian-Xun(王建勋), and Shu Guo-Xiang(舒国响)

School of Physical Electronics, University of Electronic Science and Technology of China, Chengdu 610054, *China*

(Received 6 May 2015; revised manuscript received 4 July 2015; published online 12 October 2015)

Planar Bragg reflector operating in the sub-terahertz wavelength installed at the upstream end of a sheet beam backward wave oscillator (BWO) is very promising to minimize the whole circuit structure and make it more compact. In this paper, a sub-terahertz wavelength (0.18–0.22 THz) tunable planar Bragg reflector is numerically analyzed by using multi-mode coupling theory (MCT). The operating mode TE_{10} and dominant coupling mode TE_{01} are mainly considered in this theory. Reflection and transmission performance of the reflector are demonstrated in detail and the results, in excellent agreement with the theoretical analysis and simulation, are also presented in this paper. Self- and cross-coupling coefficients between these two modes are presented as well. The reflector behaviors with different Bragg dimensions are discussed and analyzed in the 0.16–0.22 THz range. The analysis in this paper can be of benefit to the design and fabrication of the whole BWO circuit.

Keywords: planar Bragg reflector, multi-mode coupling theory, sub-terahertz BWO

PACS: 84.40.Fe, 84.40.Dc, 84.40.Az **DOI:** 10.1088/1674-1056/24/11/118403

1. Introduction

In the millimeter and sub-millimeter wavelength band, reflectors based on the Bragg coupling of counter-propagating waves in the periodic structures can provide a frequency selective feedback for overmoded high-power oscillators such as the cyclotron auto-resonance maser (CARM),[1–3] free electron laser (FEL),[4] gyrotron backward wave oscillator (BWO),[5] and terahertz (THz) BWO.[6] The periodically corrugated waveguides composed of the reflector can provide a high reflectivity through the principle of constructive interference, allowing the formation of a frequency selective resonator with effective electron beam transportation. A forward wave is coherently scattered into a reflected wave due to the cascaded corrugations. Superposition of multi-waves leads to a high reflectivity when the Bragg resonant condition ($k_b = 2k$, k is the axial propagation constant, $k_b = 2\pi/d$, and d is the corrugation period) is satisfied.

For a BWO or gyro-BWO,[5–7] the oscillation signal will be collected in the upstream end on the gun side due to the properties of the backward wave. Thus, an energy extracting system must be connected between the high-frequency slow wave structure (SWS) and the electron gun, which increases the structural complexity in the design and fabrication. One solution to this issue is to reflect the output power to the downstream end near the collector by using a Bragg reflector and then radiate it from an axially aligned horn. Like the BWO's coupling system, an input coupler for travelling wave tubes (TWTs)[8] comprised of the Bragg reflector can achieve a relatively large beam tunnel and broad bandwidth compared to the coupler with a cutoff waveguide. This structure also allows electrons to have good transportation and the path to be unobstructed. The corrugated reflector herein under discussion is very promising for realizing the compact size and miniaturizing the sheet beam BWOs or TWTs in the THz range.

Generally, a corrugated Bragg resonator with a cylindrical cross section[1,2,4,5] or coaxial structure[3,9] is adopted in the CARM, FEL, and gyro-BWO. However, a sheet electron beam promotes the development of 2D radiation sources,[10–12] where a planar Bragg reflector comprised of the symmetric periodic corrugations is of great importance for their design. A tunable planar narrow-band advanced Bragg reflector (ABR) based on the interaction between a propagating wave and a quasi-cutoff trapped wave is proposed by Ginzburg *et al.*[13,14] However, the propagating mode injected into the reflector must be in the TEM mode, which is usually not consistent with the stimulated mode in the BWO or TWT. Furthermore, the ABR width of the overmoded corrugated waveguide is very large so that high order modes may be excited. Therefore, a planar conventional Bragg reflector is considered instead of the ABR. In this paper, a planar corrugated Bragg reflector for the sub-terahertz (0.18–0.22 THz) BWO operation is demonstrated. The rest of this paper is organized as follows. In Section 2, the multi-mode coupling analysis is presented. Coupling equations of the mathematical and physical basis are derived. The formulation is similar to that for the cylindrical cross-section, and relevant reflector performances including the reflection, transmission rate and the coupling coefficients are updated by using the multi-mode coupling theory (MCT).

*Project supported by the National Natural Science Foundation of China (Grant No. G0501040161101040).

†Corresponding author. E-mail: liuguo.uestc@gmail.com

© 2015 Chinese Physical Society and IOP Publishing Ltd

In Section 3, an operating mode TE_{10} and a dominant coupling mode TE_{01} are considered. Numerical results obtained by the MCT and CST Microwave Studio (CST-MWS) are compared and their good agreement is achieved. Besides, performance based on different structural parameters is analyzed in detail and discussed, which can instruct our optimization, fabrication, and measurement in the next stage. In Section 4, conclusions are drawn from the present study.

2. Multi-mode coupling theory

Figure 1(a) shows the diagram of the BWO. In order to reflect the BWO output signal to the downstream end and then radiate it by a launching horn, a reflector comprised of corrugated waveguides is designed. Three-dimensional (3D) modeling and basic geometry of the planar Bragg reflector are configured in Figs. 1(b) and 1(c), where the right-hand side (RHS) of the reflector connects with the planar electron gun (E-gun) and the left-hand side (LHS) connects with the BWO SWS. In this figure, A^+ and A^-, respectively, represent the forward and coupling backward wave, while $A(z)$ denotes the exponentially decaying reflectivity or transmission rate. A^+ is generated by the beam-wave interaction in the BWO SWS, and then propagates towards the upstream end of the BWO due to the property of the backward wave. In the reflector, A^- is also excited due to the corrugated waveguide. Note that A^- is reflected to the SWS and then overlaps with A^+ when the Bragg resonant condition $k_b = 2k$ is satisfied, where $k = \sqrt{(\omega/c)^2 - k_c^2}$, and k_c is the cutoff wavenumber. Here we assume that the waveguide wall has a weak plane symmetric sinusoidal corrugation: $a(z) = a_0 + a_1 \cos(k_b z)$, where a_0 is the mean distance between the two corrugation plates and a_1 is the ripple amplitude. The corrugation period, width, and total longitudinal length are d, w, and l, respectively.

The coupled mode equations between A^+ and A^- can be described as[2,13]

$$\frac{dA^{\pm}}{dz} = \mp(\alpha + i\Delta)A^{\pm} \mp iGA^{\mp}. \tag{1}$$

Here, Bragg mismatch $\Delta = k - k_b/2$, α is the Ohmic dissipation loss constant (in the following discussion, we omit the influence from this item), and G is the wave coupling coefficient. Corrugations can couple one mode i to another mode j in the cavity if they satisfy the modified Bragg resonant condition

$$k_i + k_j = k_b. \tag{2}$$

The multi-mode coupling equation is

$$\frac{dA_j^{\pm}}{dz} = \mp(\alpha_j + i\Delta_j)A_j^{\pm} \mp i\sum_i G_{ij}A_i^{\mp}, \tag{3}$$

where G_{ii}, G_{jj}, and G_{ij} represent the self-coupling and cross-coupling coefficients of mode i and j, respectively. Let mode i represent a TE mode (H-mode) and mode j represent a TM mode (E-mode), then general equations will be extended to four first-order linear equations expressed in a vector form as

$$\frac{d}{dz}\begin{bmatrix} A_H^+ \\ A_H^- \\ A_E^+ \\ A_E^- \end{bmatrix} = \begin{bmatrix} -(\alpha_H + i\Delta_H) & -iG_H & 0 & -iG_X \\ iG_H & (\alpha_H + i\Delta_H) & iG_X & 0 \\ 0 & -iG_X & -(\alpha_E + i\Delta_E) & -iG_E \\ iG_X & 0 & iG_E & (\alpha_E + i\Delta_E) \end{bmatrix} \times \begin{bmatrix} A_H^+ \\ A_H^- \\ A_E^+ \\ A_E^- \end{bmatrix}, \tag{4}$$

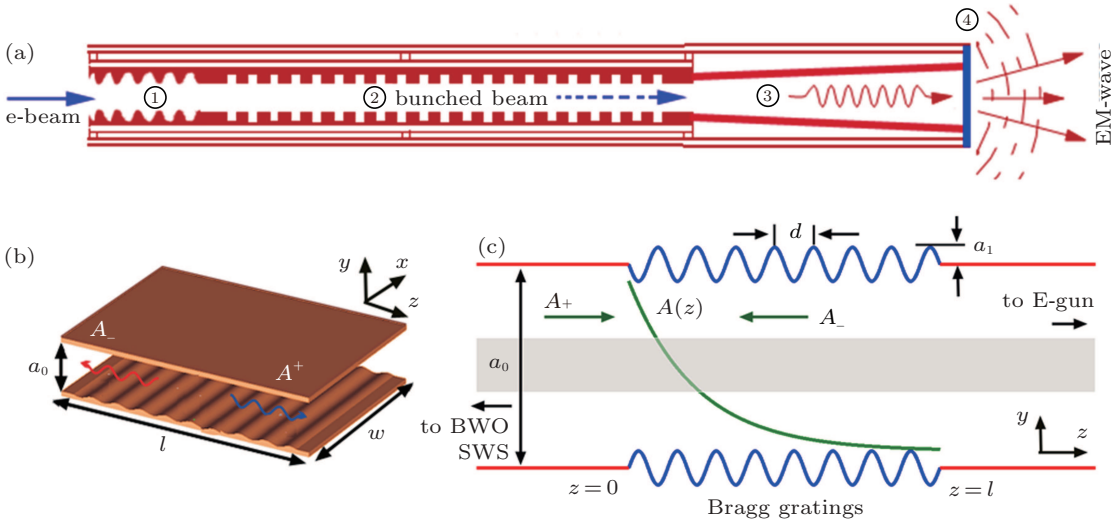


Fig. 1. (color online) (a) Backward wave oscillator with Bragg reflector. ①–④ refer to the Bragg reflector, slowing wave structures, radiation horn, and output window, respectively. (b) 3D modeling. (c) Schematic diagram of the planar Bragg reflector.

where $\Delta_{\rm H}$ and $\Delta_{\rm E}$ are the Bragg mismatch factors of the TE and TM mode; $G_{\rm H}$, $G_{\rm E}$, and $G_{\rm X}$ are the self-coupling coefficients of TE–TE and TM–TM, and cross-coupling coefficient of TE–TM, respectively.[2,15]

For a planar Bragg reflector with the consistent corrugation width discussed in this paper, the general coupling coefficients are given by[16]

$$\begin{aligned} G_{\rm H} &= \frac{a_1 N_i N_j}{4\sqrt{k_i k_j}}\left[-\xi_i^2\xi_j^2 w\varepsilon_m + \frac{mm'\pi^2}{w}\left(\frac{\omega^2}{c^2}+k_i k_j\right)\right], \\ G_{\rm E} &= \frac{a_1 M_i M_j \pi^2(\omega^2/c^2+k_i k_j)}{4\sqrt{k_i k_j}}\left(\frac{mm' a_0}{w^2}+\frac{nn' w}{a_0^2}\right), \\ G_{\rm X} &= -\frac{a_1 M_i N_j \pi^2 mn'(\omega/c)}{4a_0}\frac{(k_i+k_j)}{\sqrt{k_i k_j}}, \end{aligned} \tag{5}$$

where

$$N_{i(j)} = M_{i(j)} = \sqrt{\frac{1}{wa_0\varepsilon_{m(m')}\varepsilon_{n(n')}}}\frac{2}{\xi_{i(j)}}, \tag{6}$$

$$\xi_{i(j)} = \pi\sqrt{\frac{m(m')^2}{w^2}+\frac{n(n')^2}{a_0^2}}. \tag{7}$$

The indices i and j are for the coupling modes TE_{mn} (TM_{mn}) and $\mathrm{TE}_{m'n'}$ ($\mathrm{TM}_{m'n'}$), respectively. In these equations, $\varepsilon_p = 1$ when $p \neq 0$ and $\varepsilon_p = 2$ when $p = 0$. $G_{\rm E}$, $G_{\rm H}$, and $G_{\rm X}$ are related to the geometry a_0, a_1, w, and mode indices. If the Bragg reflector operates in a single mode, the coupling coefficients of the second self-coupling and cross-coupling items in Eq. (5) will be 0, i.e., $G_{\rm E} = 0$ and $G_{\rm X} = 0$.

The field amplitude in the waveguide satisfies $A \propto \mathrm{e}^{\lambda z}$, then equation (4) can be described as a compact matrix eigenvalue problem given by

$$(\boldsymbol{M} - \lambda \boldsymbol{I})\boldsymbol{e} = 0. \tag{8}$$

Here, matrix $\boldsymbol{M}$ is the first vector item on the RHS of Eq. (4); λ and $\boldsymbol{e}$ are its eigenvalues and eigenvectors, respectively; $\boldsymbol{I}$ is an identity matrix. Once the eigenvalues and eigenvectors are found, the amplitude vector $\boldsymbol{A}$ at any position in the reflector can be expressed as a linear combination of four eigenvectors

$$\begin{aligned} &\begin{bmatrix} \boldsymbol{A}_{\rm H}^{+}(z) \\ \boldsymbol{A}_{\rm H}^{-}(z) \\ \boldsymbol{A}_{\rm E}^{+}(z) \\ \boldsymbol{A}_{\rm E}^{-}(z) \end{bmatrix} \\ &= [K_1 K_2 K_3 K_4] \\ &\quad \times \begin{bmatrix} \boldsymbol{e}_1(1)\mathrm{e}^{\lambda_1 z} & \boldsymbol{e}_2(1)\mathrm{e}^{\lambda_2 z} & \boldsymbol{e}_3(1)\mathrm{e}^{\lambda_3 z} & \boldsymbol{e}_4(1)\mathrm{e}^{\lambda_4 z} \\ \boldsymbol{e}_1(2)\mathrm{e}^{\lambda_1 z} & \boldsymbol{e}_2(2)\mathrm{e}^{\lambda_2 z} & \boldsymbol{e}_3(2)\mathrm{e}^{\lambda_3 z} & \boldsymbol{e}_4(2)\mathrm{e}^{\lambda_4 z} \\ \boldsymbol{e}_1(3)\mathrm{e}^{\lambda_1 z} & \boldsymbol{e}_2(3)\mathrm{e}^{\lambda_2 z} & \boldsymbol{e}_3(3)\mathrm{e}^{\lambda_3 z} & \boldsymbol{e}_4(3)\mathrm{e}^{\lambda_4 z} \\ \boldsymbol{e}_1(4)\mathrm{e}^{\lambda_1 z} & \boldsymbol{e}_2(4)\mathrm{e}^{\lambda_2 z} & \boldsymbol{e}_3(4)\mathrm{e}^{\lambda_3 z} & \boldsymbol{e}_4(4)\mathrm{e}^{\lambda_4 z} \end{bmatrix}, \end{aligned} \tag{9}$$

where K_i is a constant satisfying the boundary condition. Boundaries at the reflector ends ($z = 0$ and $z = l$) for TE (TM) mode are

$$\begin{aligned} \boldsymbol{A}_{\rm H}^{+}(0) &= 1(0), \\ \boldsymbol{A}_{\rm E}^{+}(0) &= 0(1), \\ \boldsymbol{A}_{\rm H}^{-}(l) &= 0(0), \\ \boldsymbol{A}_{\rm E}^{-}(l) &= 0(0). \end{aligned} \tag{10}$$

Using the values of K_i solved by Eqs. (9) and (10), the total reflection coefficient R and total transmission coefficient T can be obtained by the combination of H- and E-mode (or H- and H-mode or E- and E-mode)

$$\begin{aligned} R &= |A_{\rm H}^{-}(0)|^2 + |A_{\rm E}^{-}(0)|^2, \\ T &= |A_{\rm H}^{+}(l)|^2 + |A_{\rm E}^{+}(l)|^2, \end{aligned} \tag{11}$$

where $|A_{\rm H}^{-}(0)|^2$ and $|A_{\rm E}^{-}(0)|^2$ are the reflected power of H- and E-modes at $z = 0$, and similarly $|A_{\rm H}^{+}(l)|^2$ and $|A_{\rm E}^{+}(l)|^2$ are the corresponding transmission power at $z = l$, where $z = 0$ and $z = l$ are the entrance (towards the SWS) and exit (towards the electron gun) of the Bragg reflector shown in Fig. 1.

3. Theoretical analysis and numerical simulation

For our sub-terahertz BWO central frequency at 0.2 THz, the designed SWS width is 1.2 mm. For simplicity, the reflector corrugation width w is also chosen as the same dimension. To make sure that the e-beam emitting from the E-gun will not be pre-bunched in the Bragg reflector and the circuit length is not too long, the mean distance between the Bragg gratings is around the dimension of the width. Considering the incident wave TE_{10} mode determined by the BWO, odd high-order modes, such as TE_{30} and TE_{50}, are not easy to generate because of the constant corrugation width. However, degenerated wave pairs TE_{10}/TE_{01} may be produced because the constant width and mean distance of the gratings are very close to each other. For our square-like overmoded corrugated waveguide with weak ripples, the 1st–2nd parasitic waves are TE_{01}, $\mathrm{TE}_{11}(\mathrm{TM}_{11})$, and TE_{20}. Two dominant modes TE_{10} and TE_{01} in the cavity controlling the reflector performance will be mainly discussed by using MCT in the following sections. With parameters of $d = 1.0$ mm, $w = 1.2$ mm, and $a_0 = 1.1$ mm, the Bragg resonance criteria $k_{\mathrm{TE}_{10}} + k_{\mathrm{TE}_{01}}$, $k_{\mathrm{TE}_{10}} + k_{\mathrm{TE(TM)}_{11}}$, $k_{\mathrm{TE}_{10}} + k_{\mathrm{TE}_{20}}$, and $k_{\rm b}$ for the fundamental TE_{10} and another coupling mode are plotted in Fig. 2. Optimal Bragg resonant points are at 0.20 THz, 0.22 THz, and 0.26 THz, respectively.

Table 1 shows a group of optimized parameters for the Bragg reflector working in a sub-terahertz band centered at 0.2 THz. Reflection, transmission performance, and self- and cross-coupling coefficients of the TE_{10}, TE_{01}, and the total combination rate obtained from MCT are demonstrated in Figs. 3(a)–3(c). The total reflection and transmission rate obtained by CST-MWS[17] are also compared in the figures. Figure 3(d) also

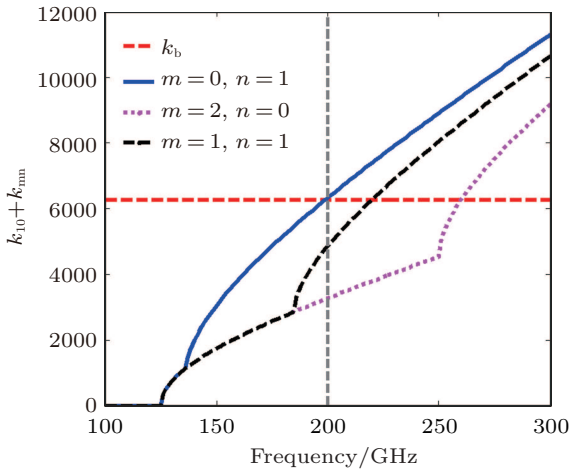


Fig. 2. (color online) Bragg resonance criteria for two modes of TE_{10} and TE_{01}, TE_{20} and $TE_{11}(TM_{11})$, where k_b is the Bragg resonant condition.

shows the total power contour plot and its normalized power flow. We can obverse that a maximum of 13.7% TE_{01} around 0.19 THz is coupled and reflected to the entrance. Total reflectivity and transmission are 0.95 and 0.05, respectively. The 3-dB bandwidths from the MCT scheme and CST-MWS are 28 GHz (0.183–0.211 THz) and 26 GHz (0.180–0.206 THz), respectively. The operating band obtained by MCT is 1%−2% higher than that from CST-MWS, which is because in our theoretical analysis only the operating mode TE_{10} and a dominant coupling mode TE_{01} are included, but much higher-order modes are neglected. From our simulation, we find the suppression to the nearest higher-order modes except the TE_{01} is maintained at a very high level (> 130 dB). We can also find that the self-coupling coefficient $G_{TE_{10}}$ increases, but the self-coupling coefficient $G_{TE_{01}}$ and cross-coupling coefficient G_X decrease with the band extending to higher frequencies. This reveals that the reflectivity in the reflector is mainly controlled by the TE_{10} mode, and this effect is enhanced with the increase of frequency.

Table 1. Typical operating parameters of the Bragg reflector.

Corrugation period	d	1.0 mm
Corrugation amplitude	a_1	0.1 mm
Corrugation width	w	1.2 mm
Mean distance	a_0	1.2 mm
Reflector length	l	8.0 mm
Center frequency	ω/ω_c	1.60

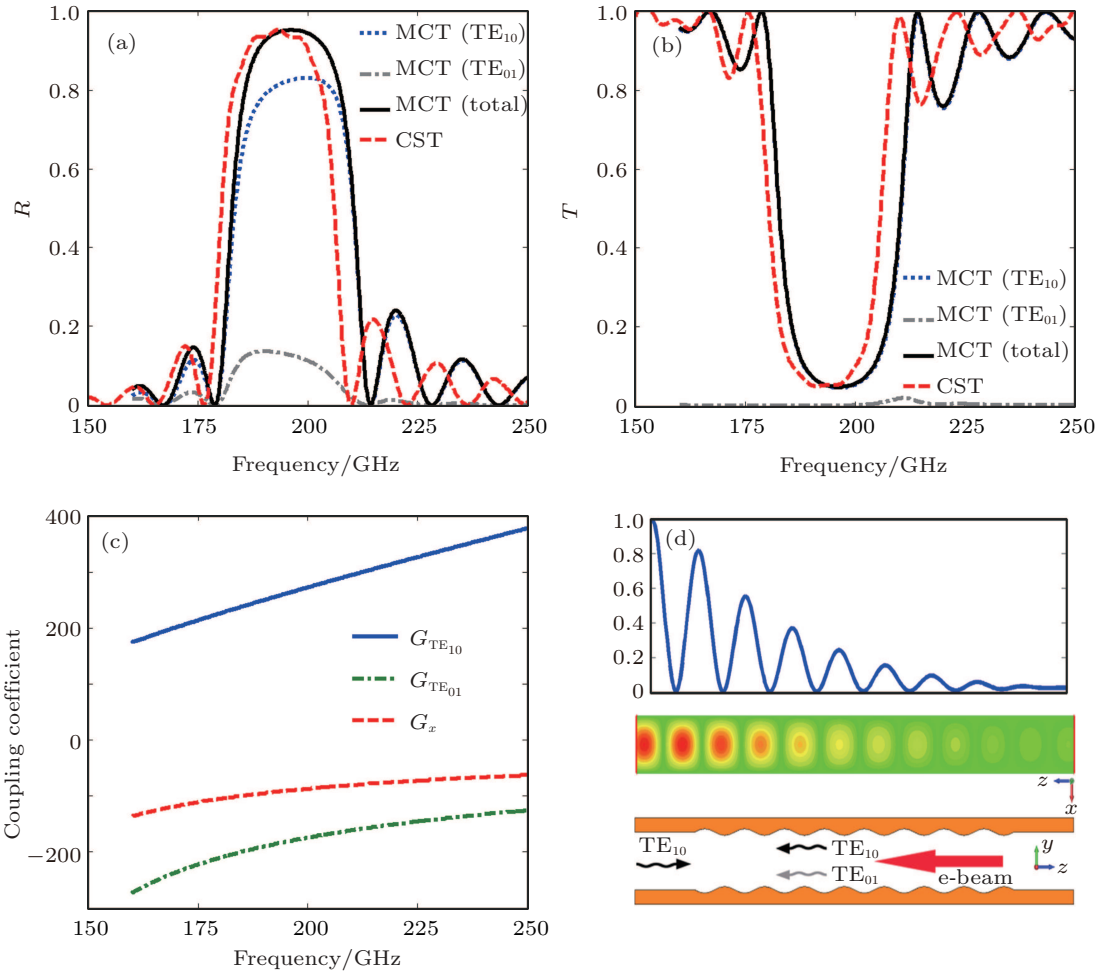


Fig. 3. (color online) Numerical results calculated by MCT and CST-MWS: (a) reflectivity and (b) transmission of TE_{10}, TE_{01}, and their combination, (c) self-coupling and cross-coupling coefficients as a function of frequencies, and (d) power distribution function and contour plot along the axial distance at 0.2 THz.

From our previous discussion and Eqs. (5)–(7), coupling coefficients are determined by the mode indices, corrugation width w, corrugation amplitude a_1, and mean distance a_0. Therefore, only the coupling coefficients relative to a_1, a_0, and w are studied in the following sections. The dependences of reflectivity, transmission, and coupling coefficients on various parameters can instruct the design, modelling, fabrication, and final tolerance assembled with our BWO slow wave structure. Figure 4 gives the reflection and transmission rates of TE_{10}, TE_{01}, and the total combination, respectively, in Figs. 4(a)–4(f), each of which is a function of the operating frequency and a_0/a_1. Our investigation indicates the reflector performances studied here, resulting from a_0 and $1/a_1$, have the same variation tendencies, thus we define a normalized factor a_0/a_1 to illustrate this situation. There are two different cases, i.e., the increasing a_0 and reducing a_1, resulting in the increase of a_0/a_1. For the former case, the increasing a_0 leads to overmoded characteristics of the corrugated waveguide so that the TE_{01} mode is much easier to excite. Both of these cases form a relatively weak ripple amplitude, which could reduce the reflectivity and bandwidth. When increasing a_0, the influence from the corrugations will be weakened and the corrugated waveguide evolves into a smooth waveguide, where TE_{10} has a very low conversion and couples with higher-order modes so that the reflector performance worsens. Figure 5 shows the relevant coupling coefficients, and one can see that the magnitudes of these coefficients reduce until they are close to zero with increasing a_0/a_1. This phenomenon is consistent with the scenarios in Figs. 4(c) and 4(f). For the distance a_0 between the two corrugations, if it is too small, the beam cross section will be limited; however, if it is too large, the confined PPM will not have enough space. From these two figures, we can also know whether the BWO is updated to a wide band operation, and reducing a_0 or increasing a_1 can improve the bandwidth of the matching Bragg reflector.

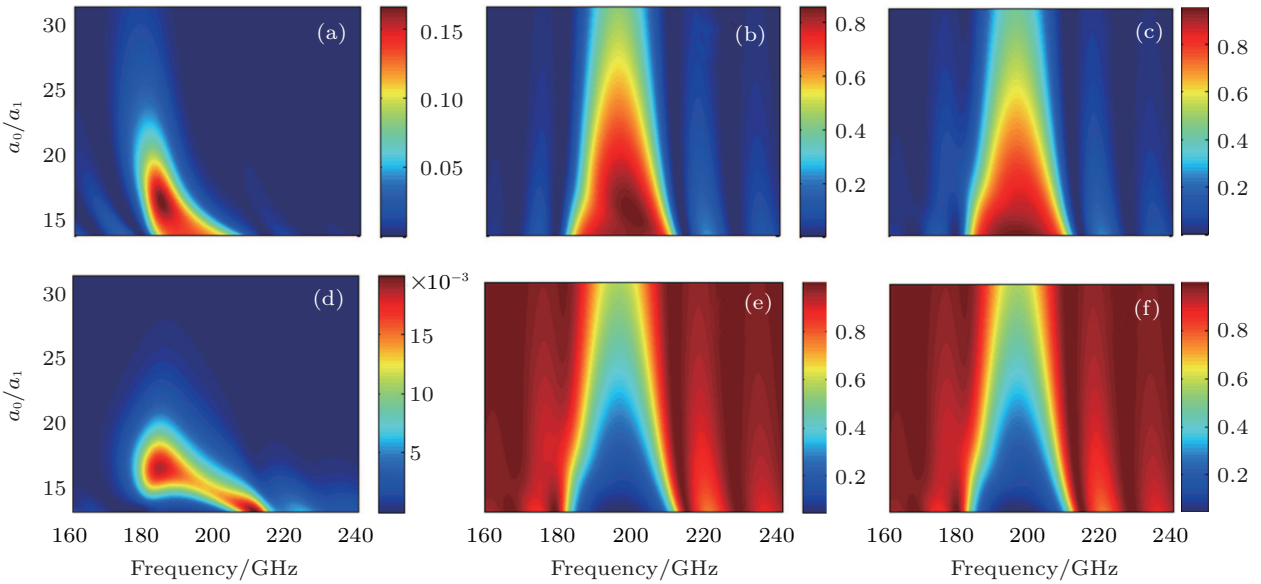


Fig. 4. (color online) Reflectivities and transmissions each as a function of frequency and normalized parameter a_0/a_1. (a)–(c) Reflectivities of TE_{01}, TE_{10}, and the total combination; and (d)–(f) transmissions of TE_{01}, TE_{10}, and the total combination.

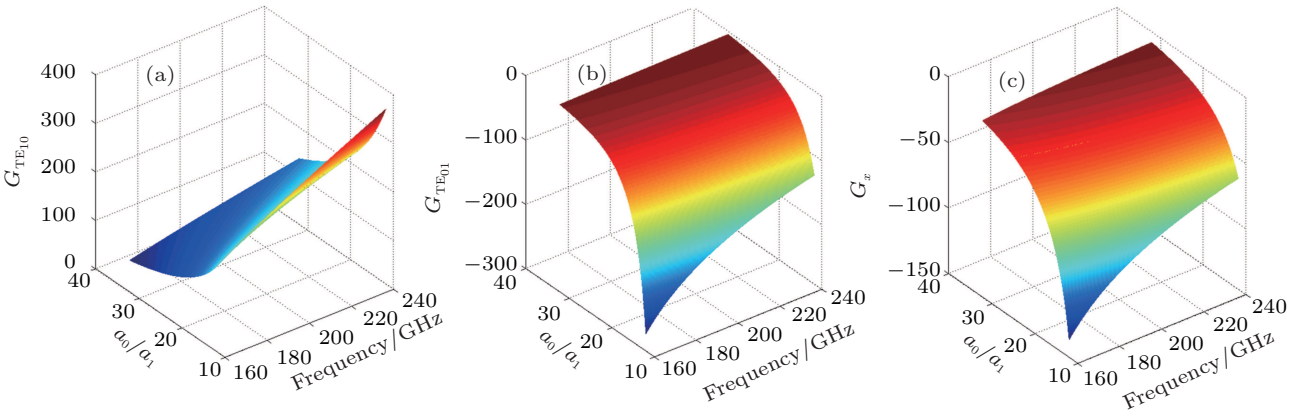


Fig. 5. (color online) (a) Self-coupling coefficient $G_{TE_{10}}$, (b) self-coupling coefficient $G_{TE_{01}}$, and (c) cross-coupling coefficient G_X versus frequency and a_0/a_1.

Figures 6 and 7, respectively, demonstrate the reflectivity, transmission rate, and coupling coefficients versus corrugation width w in the operating frequency range. When broadening w, operating bands of TE_{01}, TE_{10}, and their combination will shift to lower frequencies and meanwhile the bandwidth is greatly extended. This is because the increasing waveguide width results in a lower cutoff frequency. Note that in Figs. 6(a) and 6(d), reflection and transmission amplitudes of TE_{01} each have a concave region from $w = 1.1$ mm to 1.5 mm. Similar overmoded characteristics with the changing a_0/a_1 mentioned above occur here when changing w. Besides, the self-coupling coefficient $G_{TE_{10}}$ of TE_{10}–TE_{10} increases, and $G_{TE_{01}}$ of TE_{01}–TE_{01} remains unchanged, whereas cross-coupling coefficient G_X between TE_{10}–TE_{01} decreases. The sensitivity of the width to the reflector performance indicates that it is much easier to shift the operating band by adjusting w, but the problem is that the beam tunnel will be seriously affected.

Figures 8 and 9 demonstrate the reflectivities and transmissions each as a function of corrugation period d and normalized reflector length l/d, respectively. The reflectivity (Fig. 8(a)) of TE_{01} increases up to 0.25 when extending the corrugation period to $d = 1.5$ mm, but the stop-band center is changed to 0.16 THz. Compared with the reflectivity, its transmission (Fig. 8(d)) in this case still stays at a very low level (less than 0.06). For the combined total reflection and transmission rate shown in Figs. 8(c) and 8(f), the whole operating range also shifts to lower frequencies with increasing d, accompanied by reducing the absolute bandwidth. In Fig. 9, the reflectivities of TE_{01} and TE_{10}, respectively, concentrate in the lower and upper bands of the working range and the maximum proportions are ∼15% and 85%. Unlike the reflectivity, the proportion of TE_{01} contributing to the total transmission rate is very low in the stop band, and an interesting thing is that the maximum value (∼10%) emerges in the first side lobe but not the center. For the total reflectivity and transmission given in Figs. 9(c) and 9(f), the filtering stop bandwidth (0.18–0.22 THz) does not change except for the magnitude. If we want

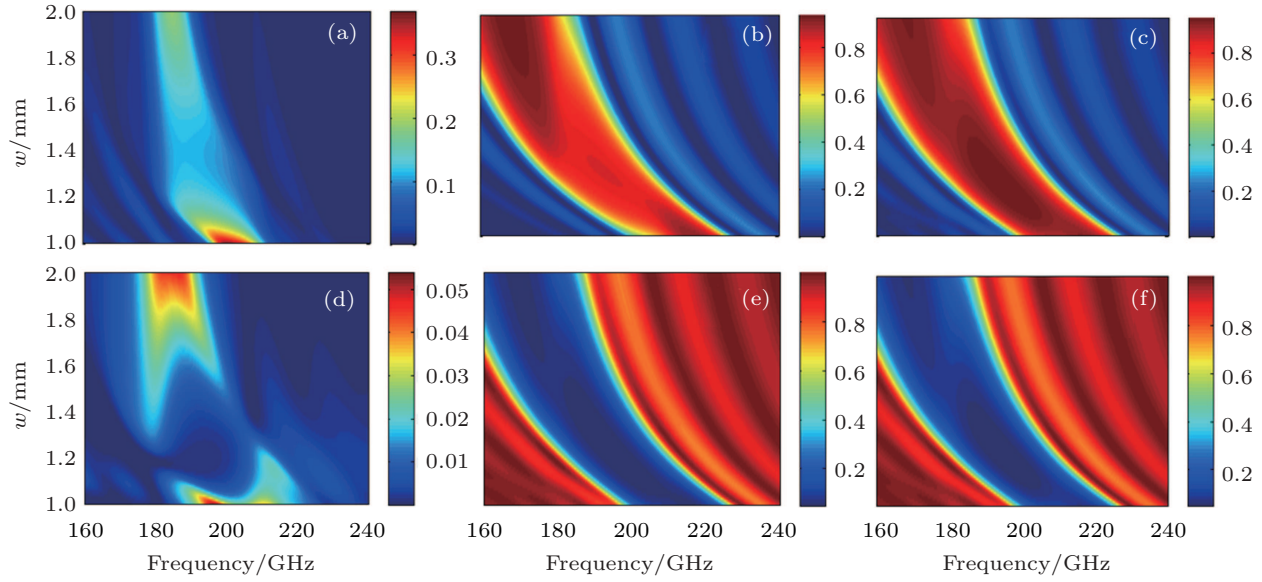


Fig. 6. (color online) Reflectivities and transmissions versus corrugation width w. (a)–(c) Reflectivities of TE_{01}, TE_{10}, and the total combination; and (d)–(f) transmissions of TE_{01}, TE_{10}, and the total combination.

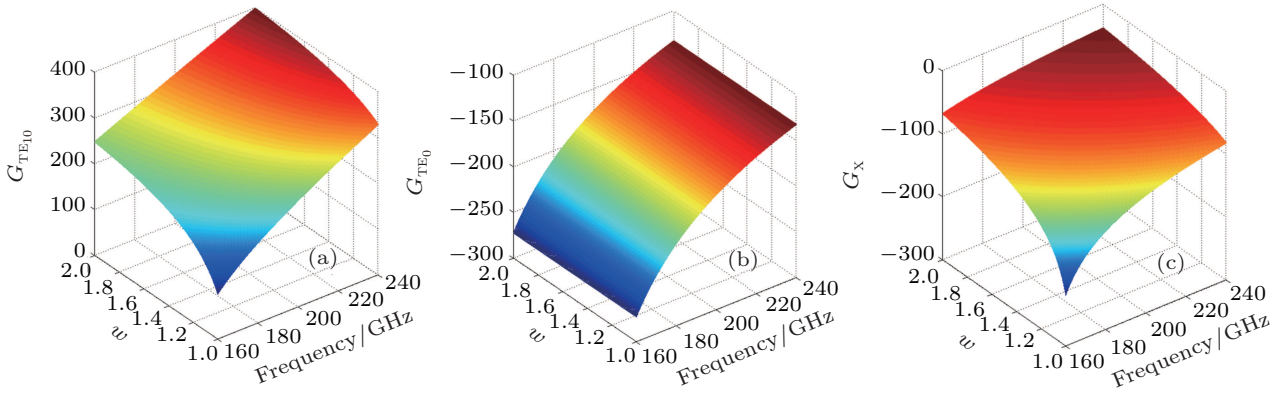


Fig. 7. (color online) (a) $G_{TE_{10}}$ for TE_{10}–TE_{10}, (b) $G_{TE_{01}}$ for TE_{01}–TE_{01}; and (c) G_X for TE_{10}–TE_{01} versus frequency and w.

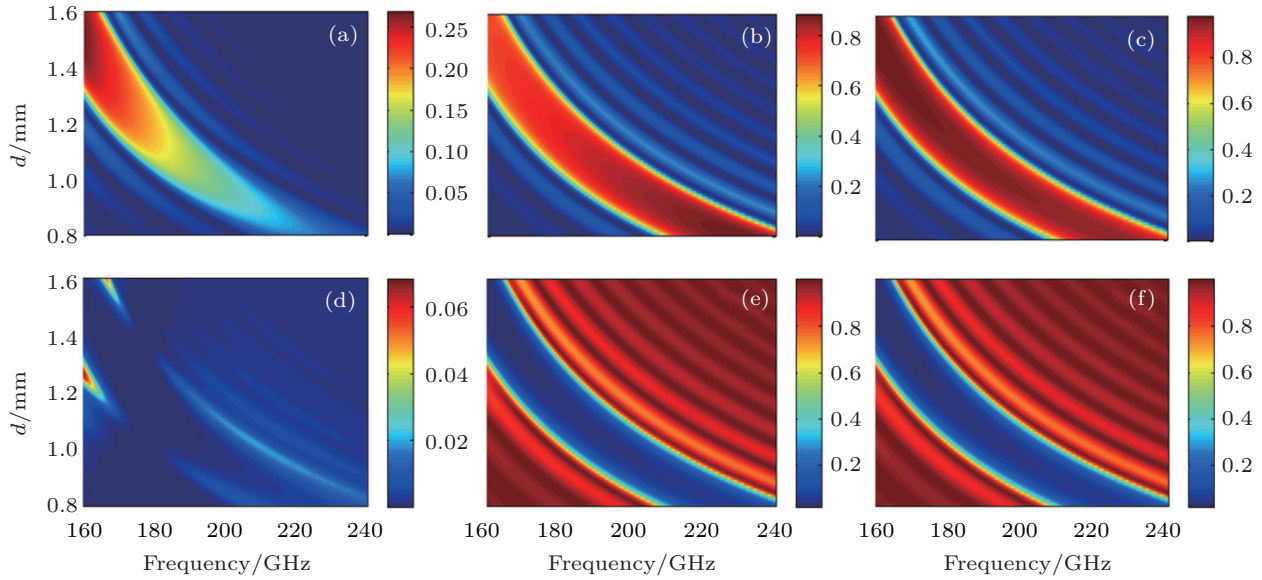


Fig. 8. (color online) Reflection and transmission rates each as a function of frequency and corrugation period d. (a)–(c) Reflectivities of TE_{01}, TE_{10}, and the total combination; and (d)–(f) transmissions of TE_{01}, TE_{10}, and the total combination.

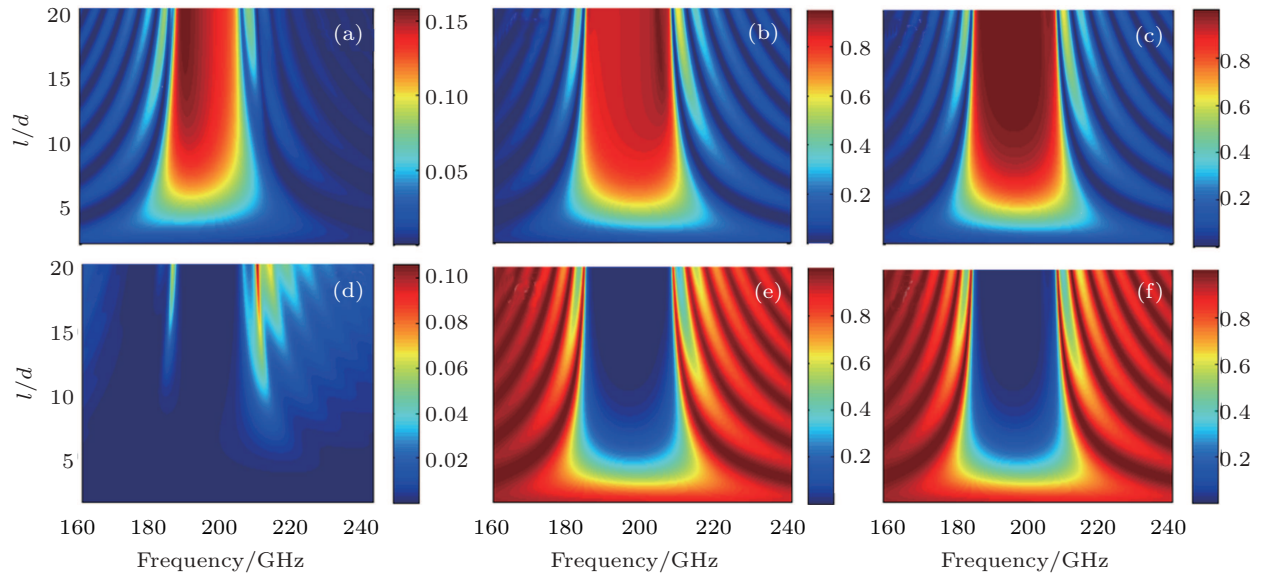


Fig. 9. (color online) Reflectivities and transmissions versus frequency and normalized reflector length l/d. (a)–(c) Reflectivities of TE_{01}, TE_{10}, and the total combination; and (d)–(f) transmissions of TE_{01}, TE_{10}, and the total combination.

to make sure that the reflectivity is over 0.95, the length of the reflector must be over 10 periodical Bragg corrugations. This conclusion can make us find the shortest reflector length so that the dimension of the whole BWO circuit is more compact in the engineering.

4. Conclusions

Multi-mode coupling theory is derived and used to analyze a sub-terahertz wavelength (0.18–0.22 THz) planar Bragg reflector, which is comprised of a periodical corrugated waveguide. It can benefit the compact design of sheet beam BWO or TWT as a promising component. A dominant mode TE_{10} and main coupling mode TE_{01} are considered in the MCT analysis. The reflector performance including reflectivity, transmission rate, and coupling coefficients calculated from MCT is examined and compared with the results obtained by CST–MWS, and good agreement is achieved. The influence of the structural dimension on reflector performance is demonstrated, which can instruct our final fabrication and assembly. The increases of a_0/a_1 and the number of Bragg cavities have no effect on the central frequency, but have great influences on the bandwidth and amplitude. Increasing the reflector width and period length would reduce the operating frequency. The bandwidth of the former case is extended, but the bandwidth of the latter one remains nearly unchanged.

References

[1] Bratman V L, Denisov G G, Ginzberg N S and Petelin M I 1983 *IEEE J. Quantum Electronics* **19** 282

[2] McCowan R B, Fliflet A W and Gold S H 1991 *NRL Memorandum Report*, February 16

[3] Xin Q, Zhang S C, Zhang H B, Kong Y Y, Chai B and Zhang Y 2010 *J. Infrared Milli. Terahz. Waves* **31** 1278

[4] Orzechowski T J, Anderson B R, Clark J C, Fawley W M, Paul A C, Prosnitz D, Scharlemann E T, Yarema S M, Hopkins D B, Sessler A M and Wurtele J S 1986 *Phys. Rev. Lett.* **57** 2172

[5] He W, Donaldson C R, Zhang L, Ronald K, McElhinney P and Cross A W 2013 *Phys. Rev. Lett.* **110** 165101

[6] Xu X, Wei Y Y, Shen F, Yin H R, Xu J, Gong Y B and Wang W X 2012 *Phys. Plasma* **19** 013113

[7] Cai J C, Hu L L, Ma G W, Chen H B, Jin X and Chen H B 2015 *Chin. Phys. B* **24** 060701

[8] Xu X, Wei Y Y, Shen F, Huang M Z, Tang T, Duan Z Y and Gong Y B 2012 *Chin. Phys. B* **21** 068402

[9] Ding X Y, Liu H and Lv Z S 2010 *J. Infrared Milli. Terahz. Waves* **31** 1156

[10] Liu G, He W, Cross A W, Yin H and Bowes D 2013 *J. Phys. D: Appl. Phys.* **46** 345102

[11] Mineo M and Paoloni C 2010 *IEEE Trans. Electron. Dev.* **57** 1481

[12] Wang Z L, Gong Y B, Wei Y Y, Duan Z Y, Zhang Y B, Yue L N, Gong H R, Yin H R, Lu Z G, Xu J and Feng J J 2013 *IEEE Trans. Electron. Dev.* **60** 471

[13] Ginzburg N S, Sergeev A S and Peskov N Y 2000 *Tech. Phys. Lett.* **26** 701

[14] Ginzburg N S, Malkin A M and Peskov N Y 2009 *Appl. Phys. Lett.* **95** 043504

[15] Chong C K, McDermott D B, Ragezhi M M, Luhmann N C, Pretterebner J, Wagner D, Thumm M, Caplan M and Kulke B 1992 *IEEE Trans. Plasma Sci.* **20** 393

[16] Katsenelenbaum B Z, Mercader L, Pereyaslavets M, Sorolla A M and Thumm M 1998 *Theory of Nonuniform Waveguides: the Cross-Section Method* (London: The Institution of Electrical Engineers) p. 159

[17] CST Corp. CST MWS Tutorials http://www.cstchina.cn/